

Structural, magnetic, and magnetocaloric properties of Fe₂CoAl Heusler nanoalloy

Aquil Ahmad^{*a}, Srimanta Mitra^{b,c}, S. K. Srivastava^b and A. K. Das^{*b}

^a*Department of Physics, School of Electrical and Electronics Engineering, SASTRA Deemed University, Thanjavur-613401, Tamilnadu, India*

^b*Department of Physics, Indian Institute of Technology Kharagpur, Kharagpur-721302, India*

^c*Space Applications Center, ISRO, Ahmedabad-380015, India*

E-mails: aquilahmad@phy.sastra.edu (A. Ahmad) and amal@phy.iitkgp.ernet.in (A. K. Das)

* *Corresponding authors.*

Abstract

Spherical nanoparticles (NPs) of size 14 ± 7 nm, made of intermetallic Fe₂CoAl (FCA) Heusler alloy, are synthesized via the co-precipitation and thermal deoxidization method. X-ray diffraction (XRD) and selected area electron diffraction (SAED) patterns confirm that the present nanoalloy is crystallized in A2-disordered cubic Heusler structure. Magnetic field (H) and temperature (T) dependent magnetization (M) results reveal that the NPs are soft ferromagnetic (FM) with high saturation magnetization (M_s) and Curie temperature (T_c). Fe₂CoAl nanoalloy do not follow the Slater Pauling (SP) rule, possibly because of the disorder present in the system. We also investigate its magnetic phase transition (MPT) and magnetocaloric (MC) properties. The peak value of $-\Delta S_M$ (entropy change) vs T curve at a magnetic field change of 20 kOe corresponds to about 2.65 J/kg-K, and the observed value of refrigeration capacity (RCP) is as large as 44 J/kg, suggesting a large heat conversion in magnetic refrigeration cycle. The Arrott plot and the nature of the universal curve accomplish that the FM to paramagnetic (PM) phase transition in Fe₂CoAl nanoalloy is of second-order. The present study suggests that the Fe₂CoAl nanoscale system is proficient, useful

and a good candidate for the spintronics application and opens up a window for further research on full-Heusler based magnetic refrigerants.

1. Introduction

A significant enhancement over conventional electronics is possible with spintronics, where aside from charge of the electron, its spin also plays an important role in order to transfer and storage of the information [1]. The numerous Heusler compounds showing half-metallic character, low Gilbert damping together with the high T_c and magnetic moment, have proven their potentiality for spintronics applications [2-5]. The scarce half-metallicity arises due to their unique electronic band structures at the fermi energy (E_F) of which one-spin (up or down) band behaves as a metal, while the other-spin (down or up) behaves as a semiconductor, and unveils an energy-gap at the E_F [3, 5]. Hence, Heusler alloys (HAs) may increase the performance of spin-based devices relying upon magnetic tunnel junction and giant magnetoresistance or spin transfer torque [6]. Quite a few materials earlier have shown up to 100% spin polarization (SP) at the E_F such as CrO_2 [7], Fe_3O_4 [8], EuS [9] and EuO [10], but most of them are neither appropriate for a high spin transport nor suitable with Si platforms because of poor electrical contacts [1, 2]. Subsequently, the hunting of novel materials for high SP is a consistently growing research field. In recent years, HAs have attracted enormous interest to the researchers due to their unique and multifunctional properties such as half-metallicity [11-14], magnetocaloric (MC) effect [15-17], thermoelectric effect [18] and catalytic behavior [19-22], shape memory effect [23], spin injection [24], and spin filtering [25]. To understand the fundamentals of MC effect, the measurement techniques for characterizing the samples and a comparative investigation of different MC materials along with probable routes to improve their performance, readers are referred to these articles [17, 26-32]. Notably, the physical properties of HAs can easily be tuned preserving their high magnetic

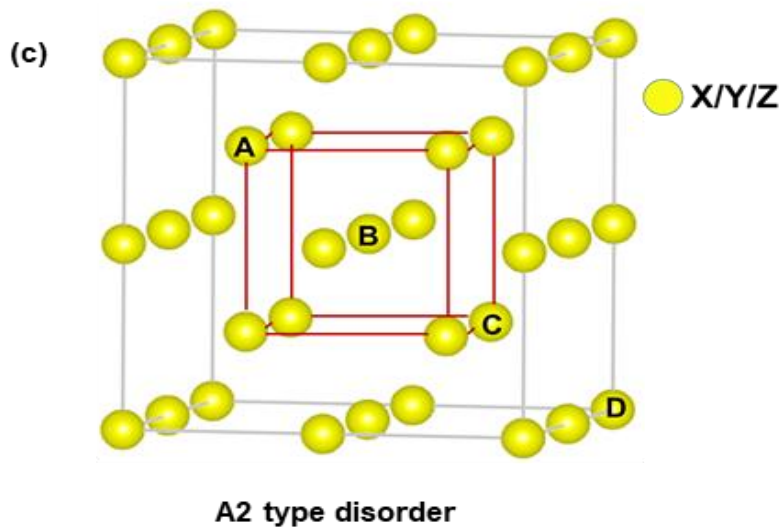
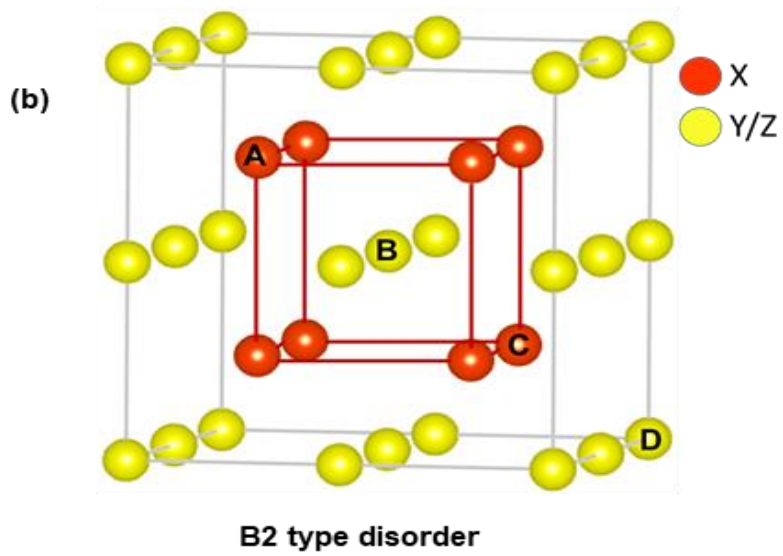
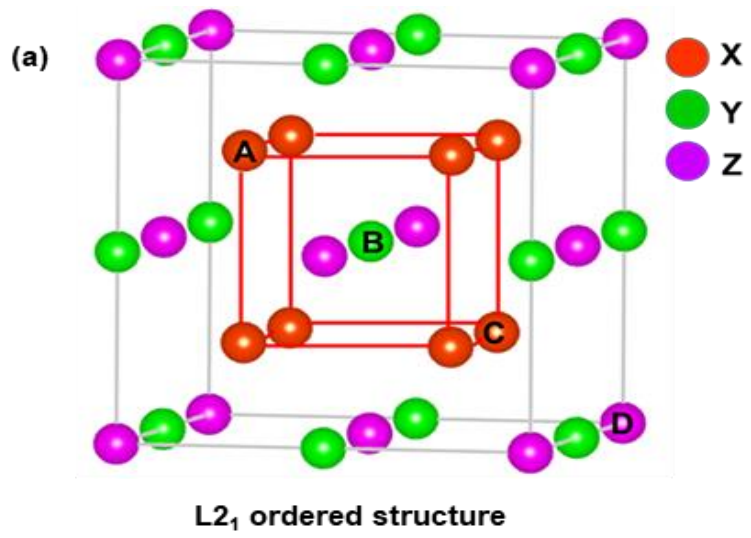


Fig. 1. Overview of most notably types of ordered/disordered crystallographic structures of X_2YZ type full Heusler compounds: (a) $L2_1$ ordered structure, (b) B2- type disordered structure, and (c) A2 type disordered (or fully disordered) structure. The four possible Wyckoff sites: A, B, C, and D are also shown in the figures. Crystal structures are generated using VESTA software.

moments and Curie temperature, by altering their elemental compositions and/or partial substitution with other elements [33-36]. X_2YZ type full Heusler compounds (X and Y: transition metals; Z: main group element) generally crystallized in highly ordered cubic $L2_1$ phase of Cu_2MnAl prototype at the room temperature. The $L2_1$ phase belongs to the $Fm\bar{3}m$ space group (#225) [6, 14, 37] and can be understood as four interpenetrating fcc sublattices of which the X atoms occupy the 8c (0.25, 0.25, 0.25 & 0.75, 0.75, 0.75) Wyckoff site, Y atoms occupy the 4b (0.5, 0.5, 0.5) site, and lastly the Z atoms reside at the 4a (0, 0, 0) site. Instead, it is frequent in literature to adopt the notation (A&C) for the sites occupied by the X atoms, (B) for the site occupied by Y atoms, and (D) for the Z atoms, as shown in Fig. 1(a). Besides ordered structure, HAs are also found to be crystallized in B2 or A2 type disordered phase. B2-disorder happens when the sites of Y and Z atoms become equivalent and forms a different cubic structure with reduced symmetry under space group $Pm\bar{3}m$, as shown in Fig. 1(b). This usually occurs in off-stoichiometric Heusler systems. A complete or A2-type disorder is observed, when all the sites of X, Y and Z atoms become equivalent. In this case, a bcc lattice is formed with reduced symmetry under space group $Im\bar{3}m$, as shown in Fig. 1(c). The ideal $L2_1$ phase can be identified experimentally, when (111) and (200) superlattice peaks are present in the XRD profile. In the case of B2 disordered phase, the (111) reflection is absent in XRD profile. Whereas, for the A2 type fully disordered structure, both the superlattice peaks (111) and (200) disappear in XRD profile [37]. A significant advancement can be seen in HAs due to new experimental approaches [38]. They are extensively studied in the form of thin films and bulk materials [39-41], although,

their study and production at the nanoscale still stay challenging [42]. The size and shape modulated nanostructures may preserve an ingenious role in multiple technological areas, as for examples: spintronics, topological insulators and skyrmionic structures [43]. Among all HAs family, Fe₂-based HAs have attracted great interest due to their high M_s and T_c [13]. The structural and electronic properties of Fe₂YAl type HAs have been intensively investigated [44-49] but their studies are very limited in nano regime, especially in Fe₂CoAl. Recently, thermoelectric property of Fe₂CoAl ribbon sample was explored [50], It exhibited a high M_s of 135 emu/g and T_c of around 1000 K along with a negative seebeck coefficient of -20 μV/K. In this article, we study the structural, magnetic and MC properties of Fe₂CoAl (FCA) nanoalloy. The powder X-ray diffraction (XRD) study suggests that FCA nanoalloy is crystallized in A2 disordered single phase, and the observed lattice constant is to be 5.74 Å. The morphological and microstructural studies reveal that the NPs are highly crystalline in nature. A relatively large value of M_s and T_c are observed in the present system; moreover, the M_s value is very stable even up to room temperature, which is desired for spintronics applications. We further systematically explore its magnetic phase transition (MPT) and MC property across the phase transition (T_c). A large peak value of the magnetic entropy change $(-\Delta S_M)_{\text{peak}}$ together with the high refrigeration capacity (RCP) and a broad working temperature range make FCA nanoalloy a potential candidate not only for spintronics but also for multistage magnetic refrigeration.

2. Experimental details

Fe₂CoAl Heusler alloy nanoparticles were synthesized using co-precipitation method as described in ref. [51] with slight modification. We have used Fe (NO₃)₃·9H₂O, CoCl₂·6H₂O, and Al₂ (NO₃)₃·18H₂O as a precursor salts, which were directly purchased from the Sigma-Aldrich. In a typical preparation of the FCA-nanoalloy, all the precursors with an appropriate molar ratio had

dissolved in 50 ml CH₃OH and dried for 10 hours at 100 °C. Thereafter, the dried powder was placed inside a tubular furnace and heated up to 850 °C for the 5 hours, in presence of H₂ environment. The crystalline phase at the room temperature was identified by high-resolution (HR) X-ray diffraction (XRD) technique using CuK α radiation ($\lambda = 1.542 \text{ \AA}$). The XRD pattern in 2θ interval from 10-100° was recorded with a step size of 0.02°. The microstructural studies were performed using field-emission scanning electron microscope (MERLIN), and HR-transmission electron microscope (TEM). The purity and composition of the elements were determined from the energy dispersive X-ray analysis (EDAX). To study the magnetic and magnetocaloric properties of FCA-NPs, the physical property measurement system (PPMS) of Cryogenics, UK and the vibrating sample magnetometer (VSM) of Lake Shore, USA with working temperature range of 5-300 K and 300-1273 K respectively, were used. In high-temperature magnetic measurements, the powder sample was placed into a disposable boron nitride (BN) cup as provided by Lake Shore, USA with the system. The isothermal magnetization vs magnetic field data were recorded for several temperatures near the magnetic phase transition temperature (T_c). Prior to the T dependent magnetization M(T) measurements, the sample was primarily cooled to 300 K from 1000 K in a zero field, which is called zero field cooled (ZFC) condition. Subsequently, data were recorded with increasing T up to 1000 K in the presence of applied field of 100 Oe.

3. Results and discussion

3.1. Microstructural, morphological and compositional analysis of Fe₂CoAl nanoalloy

The experimental and simulated X-ray diffraction patterns of FCA-NPs are shown in Fig. 2. The absence of (111) and (200) reflections in experimental curve revealed that L2₁ phase was not

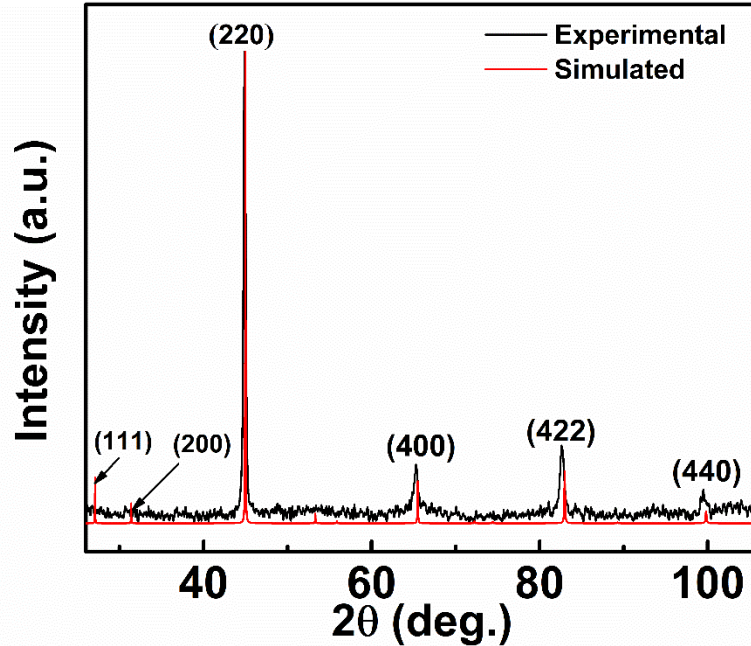


Fig. 2. The experimental and simulated x-ray diffraction pattern of FCA-NPs annealed at 850 °C for five hrs.

formed in FCA-NPs. The Bragg peaks (220), (400), (422) and (440), observed at $2\theta = 44.68^\circ$, 65.14° , 82.47° , and 99.29° , respectively, conclude that the sample was crystallized in A2-disordered phase [52]. The calculated lattice constant from the main peak of the XRD profile was found to be $a = 5.739 \pm 0.0084 \text{ \AA}$. This closely matches with the theoretical value of the bulk Fe_2CoAl [13]. It can clearly be seen from the FESEM micrograph (Fig. 3(a)) of FCA-NPs that the particles are densely agglomerated in the form of big clusters, indicating highly magnetic nature of the NPs. To check the purity and composition of the sample, we have done the EDAX analysis on NPs, as shown in Fig. 3(b). This confirms that the particles are nearly stoichiometric and pure in phase. The extra peaks are from the Si-substrate and gold coating, used at the time of sample preparation. The HRTEM image shown in Fig. 4(a) indicates that the particles are spherical in shape. The image is analyzed for particle size distribution using the ImageJ software. The histogram of size-distribution, along with the fitted Gaussian profile, is shown in Fig. 4(b).

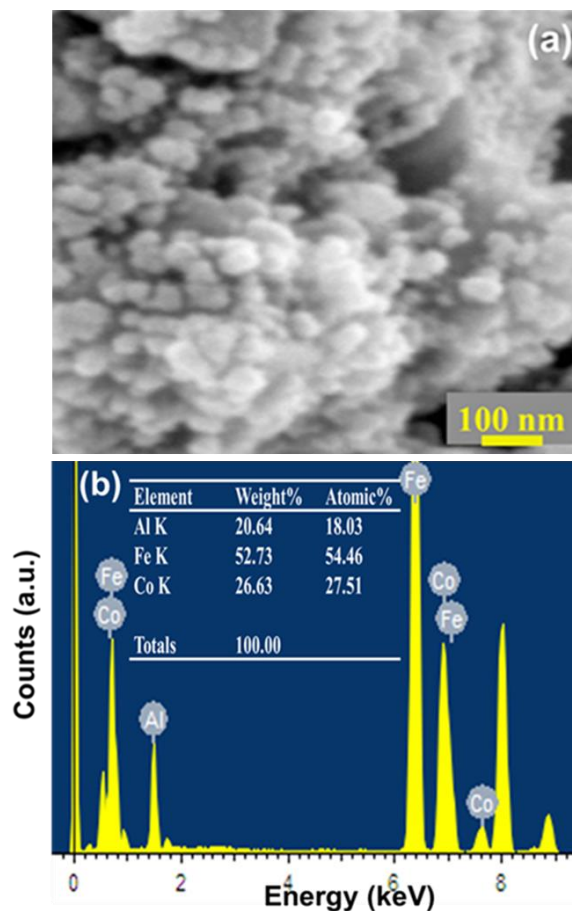


Fig. 3. (a) FESEM image of the FCA-NPs annealed at 850 °C for five hours and (b) EDAX spectrum; the inset depicts elemental composition of Fe₂CoAl nanoparticles.

According to the histogram, the NPs are of size 14 ± 7 nm. The selected area electron diffraction (SAED) pattern (Fig. 4(c)) encompassed concentric rings with dots confirms that the particles are crystalline. The first four rings are indexed with the (hkl) values (220), (400), (422) and (440), and hence are consistent with the XRD results. The image of a single particle with an even higher resolution have been shown in Fig. 4(d). The evidently visible lattice fringes confirm the high crystallinity of the particles. An enlarged portion of the image is shown in the inset of Fig. 4(d). The interplanar spacing of 2.07 \AA , as shown, is equivalent to the (220) plane of the cubic Heusler phase of Fe₂CoAl.

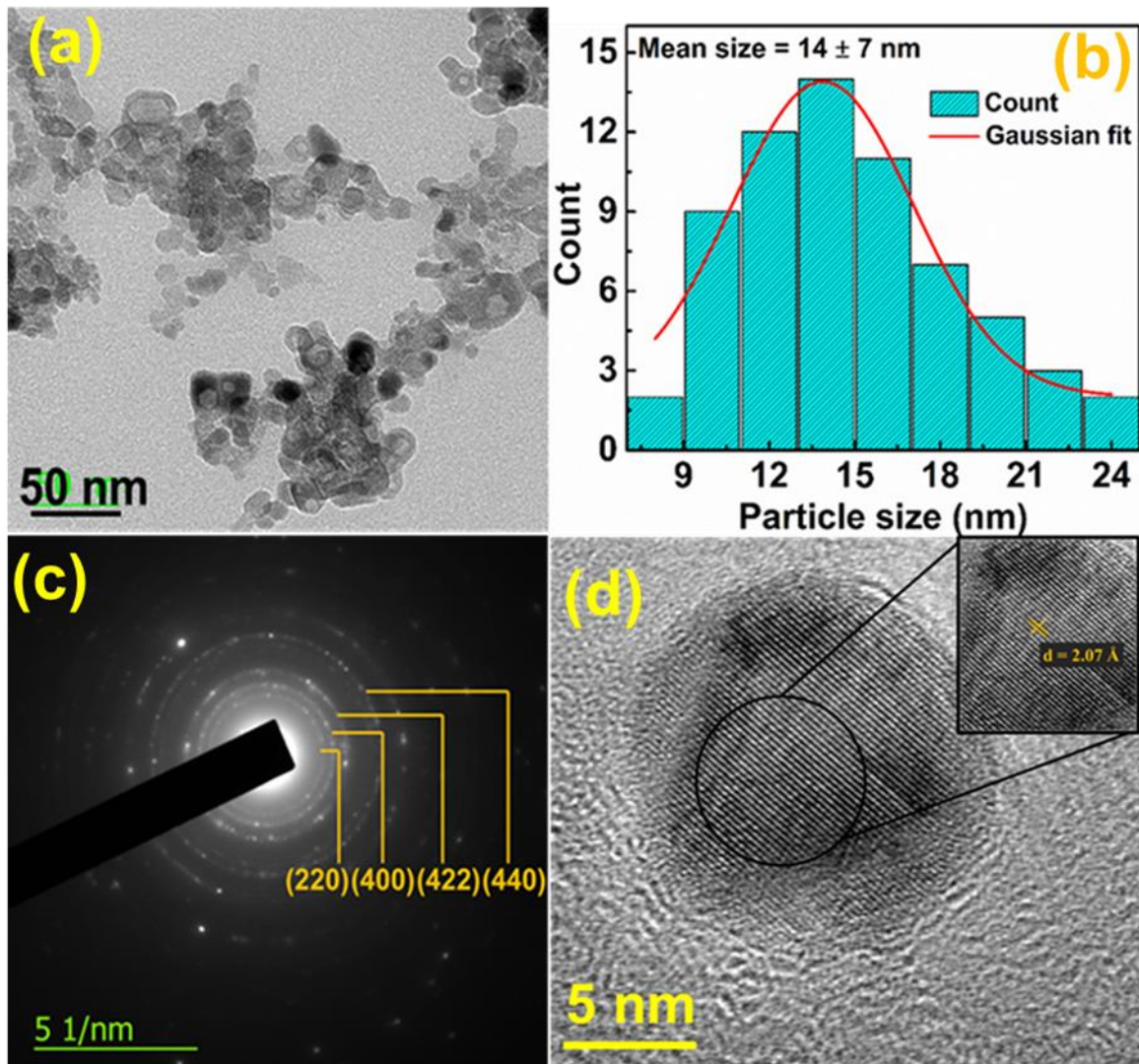


Fig. 4. (a) Transmission electron microscopy (TEM) image of the Fe_2CoAl nanoalloy. (b) Histogram of particle size. (c) SAED pattern with indexing of initial four rings. (d) High-resolution image displaying the lattice planes and crystallinity.

3.2. Magnetic behavior of Fe_2CoAl Heusler nanoalloy

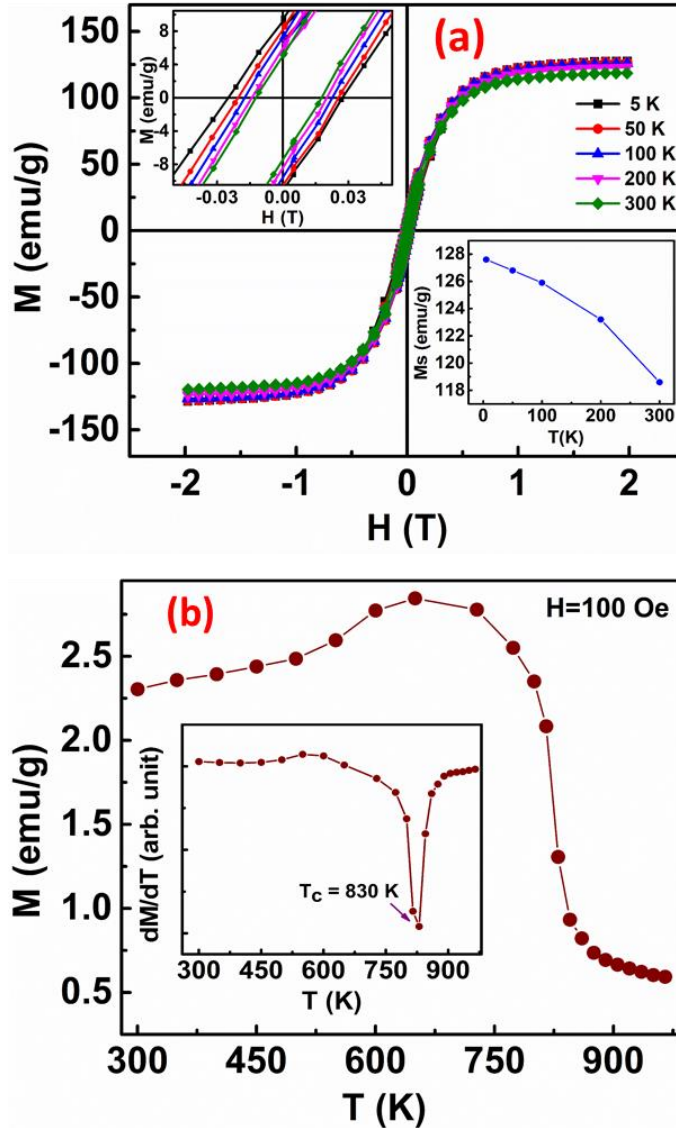


Fig. 5. (a-b) Temperature and field dependent magnetization curves of FCA-NPs; the upper and lower insets of figure 5(a) show the magnified version near the zero field region and the variation of saturation magnetization with temperature, respectively. Inset of figure 5(b) shows the dM/dT vs T curve.

The field-dependent magnetization $M(H)$ curves at different temperatures starting from 5 to 300 K are shown in Fig. 5(a). The low-temperature (5 K) M_s was found to be 127.6 emu/g and converted into $4.5 \mu_B/\text{f.u.}$ This is larger than the Slater Pauling (SP) value of $4 \mu_B/\text{f.u.}$ [53], and slightly less than the bulk value as reported by V. Jain et al. [54]. The reason of deviation from the

SP value might be due to the disorder present in this nanometric sample. As evident from the inset of M (H) curve, the finite value of the coercivity (H_c) and the remanence (M_r) is indicating ferromagnetic behavior of the NPs. A comparison of all the values of M_s , M_r , and H_c is tabulated in Table 1. The T dependence of the M_s curve, the lower inset of Fig. 5(a), reveals that M_s is stable even up to room temperature, which is good for spintronics application. The temperature dependent magnetization, M (T) curve at the applied field of 100 Oe, under zero field-cooled condition (ZFC) is shown in Fig. 5(b). M is increased with respect to the T and reached maximum at 650 K. The ZFC curve of FCA-NPs was smooth and show a clear FM to PM phase transition at the T_c . We have also measured the M (T) curve under field cooled (FC) condition (not shown here) and found no significant thermal hysteresis in ZFC-FC curves of FCA-NPs, which suggests that the phase transition is of second-order [55]. The T_c was calculated from the first derivative of M (T) versus T curve (see inset of figure 5(b)), and was found to be 830 K.

3.3. Magnetocaloric properties of Fe₂CoAl Heusler nanoalloy

To analyze the MC properties of FCA-NPs, isothermal magnetization curves in field increasing (0 Oe-20 kOe) mode, were recorded at various temperatures from 795-851 K with a temperature interval of 4 K, across the T_c , as shown in Fig. 6(a). The increasing nature of the magnetization up to 5 kOe subsequently becomes constant, and then decreases with respect to the

Temperature (K)	Sat. magn. M_s (emu/g)	Remanence M_r (emu/g)	Coercivity H_c (Oe)	Curie temperature (K)
5	127.6	9.2	259	830 [this work]
50	126.8	8.2	229	990 [50]
100	125.9	7.3	200	
200	123.2	5.9	171	
300	118.6	5.0	150	
Bulk Sat. magn.			4.7 μ_B /f.u. [54]	
Slater Pauling M_s value			4.0 μ_B /f.u. [53]	

Table 1. Temperature dependence of M_s , M_r , H_c , and T_c of FCA-NPs; other theoretical and experimental values are also tabulated for a comparison.

temperature increment indicating a magnetic transition from FM to PM phase. Moreover, a huge change of the magnetization in the temperature range of 827-831 K suggests a large MC effect in FCA-NPs. Here we did not find any significant magnetic hysteresis with field decreasing (20 kOe - 0 Oe) mode (not shown here). This reversible nature of magnetic phase transition is vital for magnetic refrigeration. Arrott plot or M^2 versus H/M curve [56] was also constructed, to check if the Landau mean field theory for the MPT is suitable for FCA-NPs, as shown in Fig. 6(b).

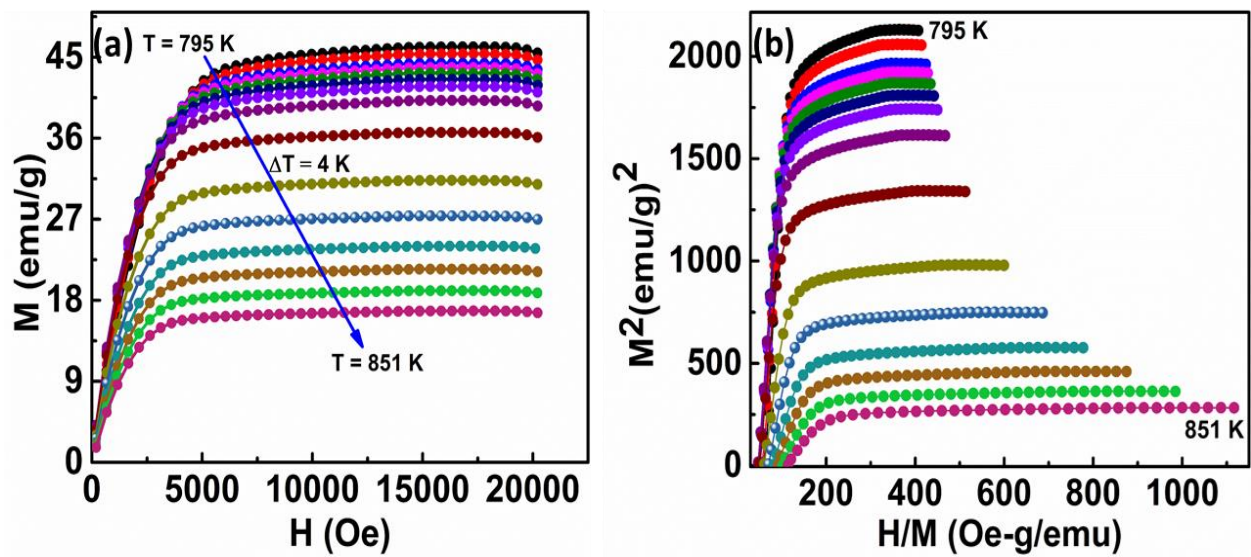


Fig. 6. (a) $M(H)$ curves of Fe_2CoAl Heusler alloy nanoparticles measured around the phase transition and (b) Arrott curve of the isotherms near the T_c .

It is widely accepted that the conventional Arrott curves would exhibit parallel straight lines for the critical exponents of $\gamma = 1$ and $\beta = 0.5$, and the critical temperature (T_c) will be defined exactly at the line which passes through the origin. The downward curvature along with the nonlinear behavior even at high-field region was observed. Apparently, we conclude that the mean field theory of phase transition is not valid in present system and a complex behavior of the critical

exponents near the T_c is expected. Moreover, the positive slope of Arrott plot following Banerjee's criterion [57] indicates FM to PM phase transition is of second order. The change in magnetic entropy ($-\Delta S_M$) was calculated using Maxwell equation [58]:

$$\Delta S_M = S(T, H) - S(T, 0) = \int_0^H \left(\frac{\partial M}{\partial T} \right)_H dH \quad (1)$$

The T dependence of magnetic entropy change ($-\Delta S_M$) is presented in Fig. 7. A positive anomaly in $-\Delta S_M$ vs T curve was observed at 830 K, which is much closer to its T_c . The maxima in the change in magnetic entropy vs temperature curve at a magnetic field of 20 kOe corresponds to about 2.65 J/Kg-K. It is clear from the inset of Fig. 7 that the peak value of the magnetic entropy change, $(-\Delta S_M)_{\text{peak}}$ increases linearly with temperature; therefore, a large value of $-\Delta S_M$ is

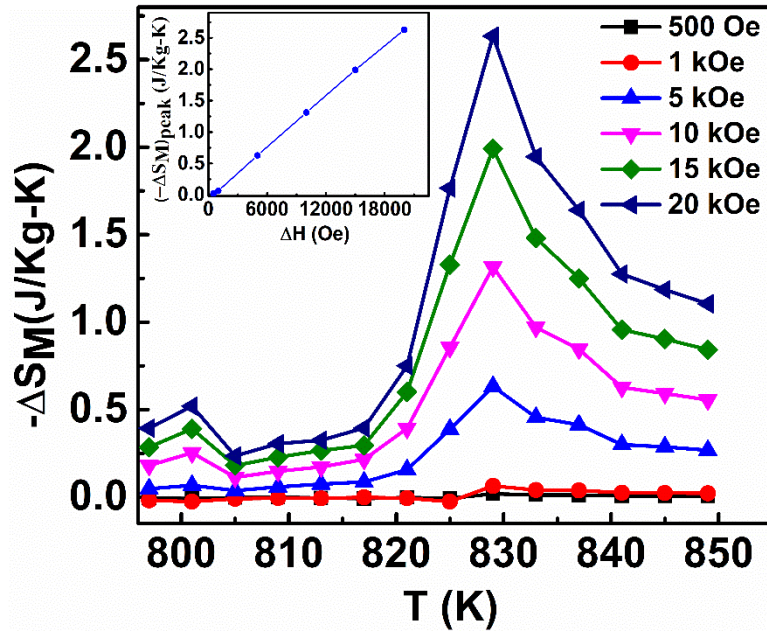


Fig. 7. $-\Delta S_M$ versus temperature curve for Fe_2CoAl Heusler nanoalloy; The inset shows the change of $(-\Delta S_M)_{\text{peak}}$ value with respect to the changing field (ΔH).

expected for higher fields but we could not measure it due to the temperature limitation of our system. The usefulness of magnetic refrigerants can be evaluated by a parameter: relative cooling

power (RCP), which measures the amount of heat transferred between hot and cold reservoirs and is defined as $RCP = -(\Delta S_M)_{peak} \times \Delta T_{FWHM}$, where ΔT_{FWHM} denotes the full-width at half-maximum of the change in $-\Delta S_M$ vs T curve [59]. ΔT_{FWHM} also represents the span of working-temperature in the system, which was found to be around 17 K; such broad working temperature range is highly desired for magnetic refrigeration. As Engelbrecht *et al.* [60] previously suggested that a material having a broad peak of $-\Delta S_M$ is much better than that of materials with a sharp peak of magnetic entropy change for cooling applications and therefore, such materials with broad temperature

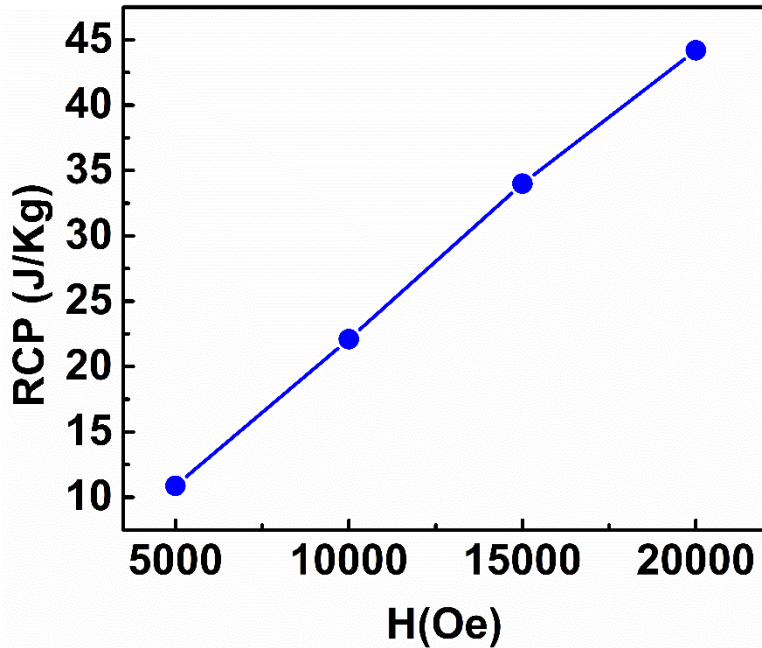


Fig. 8. Field dependence of the relative cooling power (RCP) across the phase transition (T_c)

distribution, are much attractive for MC application. The observed value of RCP is as large as 44 J/Kg at the magnetic field change of 20 kOe, suggesting a large heat conversion in magnetic refrigeration cycle. As observed from the inset of Fig. 7, and Fig. 8, both the change in magnetic entropy and RCP values have shown a linear dependence with the applied field in the range of 0-20 kOe. This increasing nature of $(-\Delta S_M)_{peak}$ and RCP with ΔH along with the broader working

temperature range would be suitable for Ericsson-cycle refrigeration application [61]. Thus exploitation of magnetic and magnetocaloric properties in Fe₂-based Heusler nanoalloys may be useful for not only spintronics but also for multistage magnetic refrigeration technology [34, 62]. A comparison of these values with previous magnetic refrigerants is presented in Table 2.

Materials		$-\Delta S_M$ (J/Kg -K)	Working temperature span, ΔT_{FWHM} (K)	RCP (J/Kg)	Field range (ΔH) in kOe	T_c (K)	Nature of the Phase transiti on	Refs.
Heusler nanoparticles	Fe ₂ CoAl	2.65	17	44	20	830	Second -order	present work
	Co ₂ FeAl	15	6	89	14	1261	Second -order	[17]
Bulk Heusler alloys	Mn _{1-x} Cr _x Co	~28.5	—	—	50	322	First- order	[63]
	Ge							
	MnCo _{1-x} Zr _x Ge	7.2	—	266	50	274	First- order	[64]
	Mn _{1-x} Al _x CoGe	12	—	303	50	286	First- order	[65]
	Co ₂ Cr _{0.25} Mn _{0.75} Al	3.5	—	285	90	720	Second -order	[34]

Table 2. A comparison of the $(-\Delta S_M)_{\text{peak}}$, RCP, ΔT_{FWHM} , ΔH , T_c , and nature of the phase transition in Fe₂CoAl nanoalloy and other MC materials.

In Co₂FeAl Heusler NPs [66], we have observed a giant magnetocaloric effect around 1252 K. However, such a high T_c and sharp peak in $(-\Delta S_M)_{\text{peak}}$ vs temperature curve make it less efficient for magnetic refrigeration. This further opens a way of hunting the new Heusler compounds, especially, in nano regime. Our $(-\Delta S_M)_{\text{peak}}$, value is higher than that of the Co₂Cr_{0.25}Mn_{0.75}Al (Table 2), and RCP value is at least comparable on the same field scale. The present values are also considerably larger than that of the other Co₂-based full Heusler alloys [67]. On the contrary, a huge RCP value of 400 J/Kg at 50-kOe magnetic field was reported in Gadolinium [68]. Nevertheless, it is not suitable for commercial purposes due to its high cost, and therefore Ni-based Heusler compounds [69-72] are extensively investigated for better performing magnetocaloric effect in recent years. Though, most of them exhibit a first-order phase transition causing a thermal and magnetic hysteresis near the T_c . The present MC study suggests that the Fe₂CoAl nanoalloy might be suitable for multistage magnetic refrigeration technology and further opens a window of research on how its magnetic and magnetocaloric properties can be tuned by size and shape modulation of the nanoparticles, which we aim in our future work. A master curve or universal curve was proposed by Franco et al. [73] for the MC materials exhibiting second-order phase transition near the T_c . The curve was defined as the normalized entropy change $\Delta S'_M$ with respect to rescaled temperature (θ) where $\Delta S'_M = \Delta S_M / \Delta S_M^{\text{peak}}$ and θ defined as:

$$\theta = \left\{ \begin{array}{l} \frac{-(T-T_c)}{(T_{r1}-T_c)}, \text{ for } T \leq T_c; \\ \frac{(T-T_c)}{(T_{r2}-T_c)}, \text{ for } T > T_c \end{array} \right\} \quad (2)$$

In above equation, Curie temperature (T_c) denotes the temperature at the peak value of the magnetic entropy change (ΔS_M^{peak}). Reference temperatures T_{r1} and T_{r2} were taken as the temperatures analogous to $\frac{1}{2} \Delta S_M^{\text{peak}}$ below and above the Curie temperature (T_c). As seen from Fig. 9, $\Delta S'_M$ vs θ curves of FCA-NPs, taken at different applied fields, have been merged into a single universal curve, which confirms a second order magnetic phase transition across the T_c .

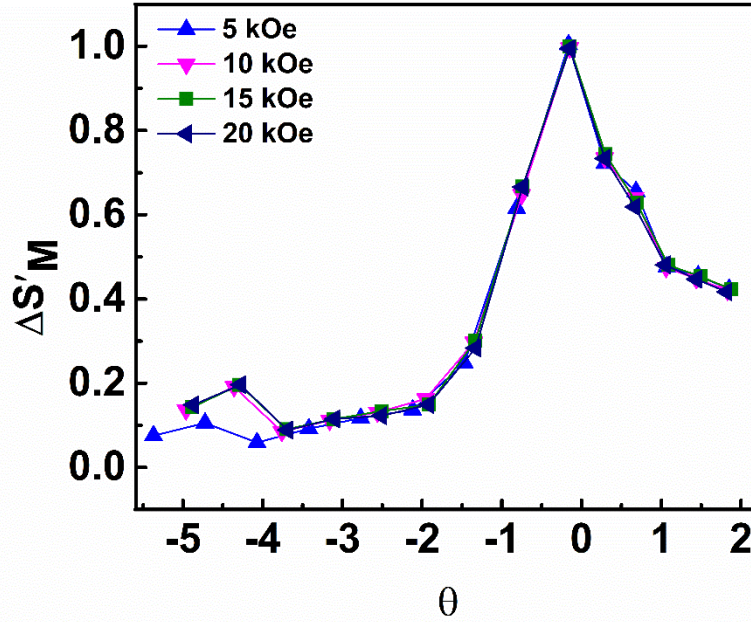


Fig. 9. The magnetic entropy ($\Delta S'_M$) as a function of rescaled temperature (θ) near T_c for Fe_2CoAl Heusler nanoalloy.

Such behavior of phenomenological curves was observed previously in second-order phase transition materials [66, 73, 74]. This study recommends of using this large MC material with a broad working temperature range in magnetic refrigeration, as in multi-stage magnetic refrigeration where cooling from high temperature is desired in more than one stages [75]. Such multi-stage magnetic refrigerators are highly appropriate for industrial application, where the low temperature of one stage acts as upper temperature for the next stage [26, 75].

4. Conclusions

Fe_2CoAl Heusler nanoparticles of size 14 nm were grown using co-precipitation method. The microstructure of the NPs was examined by XRD, FESEM, HRTEM, and SAED. Structural characterizations confirmed the crystalline nature of particles with A2-disorder, and uniform

chemical distribution of the elements. The magnetic characterization on the FCA-NPs supports their soft ferromagnetic character with high M_s of about 127.6 emu/g (or 4.5 μ_B /f.u.) and high T_c of 830 K. The peak value of the change in magnetic entropy ($-\Delta S_M$) vs temperature curve at a magnetic field of 20 kOe corresponds to about 2.65 J/Kg-K, and the observed value of refrigeration capacity (RCP) is as large as 44 J/Kg. To analyze the MPT, a detailed analysis of magnetization is performed. The Arrott plot and the nature of the universal curve accomplish that the FM-PM phase transition is of second order.

Notes: The authors declare no competing financial interest.

Acknowledgements:

Aquil Ahmad acknowledges the University Grants Commission, New Delhi and Ministry of Education (MoE), India for providing the research fellowship. A. Ahmad also acknowledges the Central Research Facility (CRF), and the Departmental lab facility of IIT Kharagpur, India for the sample characterizations and DFT computations. A K Das acknowledges the financial support from the Department of Science and Technology (DST), India (Project No. EMR/2014/001026).

References

- [1] J.P. deGrave, A.L. Schmitt, R.S. Selinsky, J.M. Higgins, D.J. Keavney, S. Jin, Spin Polarization Measurement of Homogeneously Doped $Fe_{1-x}Co_xSi$ Nanowires by Andreev Reflection Spectroscopy, *Nano Lett.* 11 (2011) 4431-4437.
- [2] M. Jourdan, J. Minár, J. Braun, A. Kronenberg, S. Chadov, B. Balke, A. Gloskovskii, M. Kolbe, H.J. Elmers, G. Schönhense, Direct observation of half-metallicity in the Heusler compound $Co_2 MnSi$, *Nat. Commun.* 5 (2014) 1-5.
- [3] C. Felser, L. Wollmann, S. Chadov, G.H. Fecher, S.S. Parkin, Basics and prospective of magnetic Heusler compounds, *APL Materials* 3 (2015) 041518.

- [4] S. Idrissi, R. Khalladi, S. Ziti, N. El Mekkaoui, S. Mtougui, H. Labrim, I. El Housni, The electronic and magnetic properties of the rare earth-based quaternary Heusler compound LuCoVGe, *Physica B: Cond. Matter* 562 (2019) 116-123.
- [5] T. Graf, C. Felser, S.S.P. Parkin, *Heusler Compounds: Applications in Spintronics*, Springer (2016) pp 335-364, https://doi.org/10.1007/978-94-007-6892-5_17.
- [6] T. Graf, C. Felser, S.S. Parkin, Simple rules for the understanding of Heusler compounds, *Progress Solid State Chem.* 39 (2011) 1-50.
- [7] K. Kämper, W. Schmitt, G. Güntherodt, R. Gambino, R. Ruf, CrO₂—A New Half-Metallic Ferromagnet?, *Phys. Rev. Lett.* 59 (1987) 2788.
- [8] Y.S. Dedkov, U. Rüdiger, G. Güntherodt, Evidence for the half-metallic ferromagnetic state of Fe₃O₄ by spin-resolved photoelectron spectroscopy, *Phys. Rev. B* 65 (2002) 064417.
- [9] R.S. Selinsky, D.J. Keavney, M.J. Bierman, S. Jin, Element-specific magnetometry of EuS nanocrystals, *Appl. Phys. Lett.* 95 (2009) 202501.
- [10] M.J. Bierman, K.M. Van Heuvelen, D. Schmeisser, T.C. Brunold, S. Jin, Ferromagnetic semiconducting EuO nanorods, *Advanced Materials* 19 (2007) 2677-2681.
- [11] I. Galanakis, P. Dederichs, N. Papanikolaou, Slater-Pauling behavior and origin of the half-metallicity of the full-Heusler alloys, *Phys. Rev. B* 66 (2002) 174429.
- [12] A. Ahmad, S. Srivastava, A. Das, Phase stability and the effect of lattice distortions on electronic properties and half-metallic ferromagnetism of Co₂FeAl Heusler alloy: An ab initio study, *J. Phys.: Condens. Matter* 32 (2020) 415606.
- [13] A. Ahmad, A.K. Das, S.K. Srivastava, Competition of L2₁ and XA ordering in Fe₂CoAl Heusler alloy: a first-principles study, *Eur. Phys. J. B* 93 (2020) 1-7.
- [14] A. Ahmad, S. Srivastava, A. Das, Effect of L2₁ and XA ordering on phase stability, half-metallicity and magnetism of Co₂FeAl Heusler alloy: GGA and GGA+U approach, *J. Magn. Magn. Mater.* 491 (2019) 165635.
- [15] X. Zhang, H. Zhang, M. Qian, L. Geng, Enhanced magnetocaloric effect in Ni-Mn-Sn-Co alloys with two successive magnetostructural transformations, *Scientific Reports* 8 (2018) 1-11.
- [16] T. Krenke, E. Duman, M. Acet, E.F. Wassermann, X. Moya, L. Mañosa, A. Planes, Inverse magnetocaloric effect in ferromagnetic Ni–Mn–Sn alloys, *Nature Materials* 4 (2005) 450-454.

- [17] A. Ahmad, S. Mitra, S.K. Srivastava, A.K. Das, Giant magnetocaloric effect in Co_2FeAl Heusler alloy nanoparticles, *J. Physics D: Appl. Phys.* 54 (2021) 385001.
- [18] T. Graf, J. Barth, B. Balke, S. Populoh, A. Weidenkaff, C. Felser, Tuning the carrier concentration for thermoelectrical application in the quaternary Heusler compound $\text{Co}_2\text{TiAl}_{(1-x)}\text{Si}_x$, *Scripta Materialia* 63 (2010) 925-928.
- [19] T. Kojima, S. Kameoka, A.P. Tsai, The emergence of Heusler alloy catalysts, *Scie. Techn. Advanced Materials* 20 (2019) 445-455.
- [20] T. Kojima, S. Kameoka, S. Fujii, S. Ueda, A.-P. Tsai, Catalysis-tunable Heusler alloys in selective hydrogenation of alkynes: A new potential for old materials, *Science Advances* 4 (2018) eaat6063.
- [21] T. Kojima, S. Kameoka, A.-P. Tsai, Catalytic Properties of Heusler Alloys for Steam Reforming of Methanol, *ACS Omega* 4 (2019) 21666-21674.
- [22] T. Kojima, S. Kameoka, A.-P. Tsai, Heusler alloys: A group of novel catalysts, *ACS Omega*, 2 (2017) 147-153.
- [23] P. Devi, M.G. Zavareh, C.S. Mejía, K. Hofmann, B. Albert, C. Felser, M. Nicklas, S. Singh, Reversible adiabatic temperature change in the shape memory Heusler alloy $\text{Ni}_{2.2}\text{Mn}_{0.8}\text{Ga}$: An effect of structural compatibility, *Phys. Rev. Mater.* 2 (2018) 122401.
- [24] S. Datta, B. Das, Electronic analog of the electro-optic modulator, *Appl. Phys. Lett.* 56 (1990) 665-667.
- [25] K. Kilian, R.H. Victora, Electronic structure of Ni_2MnIn for use in spin injection, *J. Appl. Phys.* 87 (2000) 7064-7066.
- [26] V. Franco, J. Blázquez, J. Ipus, J. Law, L. Moreno-Ramírez, A. Conde, Magnetocaloric effect: From materials research to refrigeration devices, *Progress Materials Science* 93 (2018) 112-232.
- [27] B. Wu, Y. Zhang, D. Guo, J. Wang, Z. Ren, Structure, magnetic properties and cryogenic magneto-caloric effect (MCE) in $\text{RE}_2\text{FeAlO}_6$ (RE= Gd, Dy, Ho) oxides, *Ceramics International* 47 (2021) 6290-6297.
- [28] L. Li, P. Xu, S. Ye, Y. Li, G. Liu, D. Huo, M. Yan, Magnetic properties and excellent cryogenic magnetocaloric performances in B-site ordered $\text{RE}_2\text{ZnMnO}_6$ (RE= Gd, Dy and Ho) perovskites, *Acta Materialia* 194 (2020) 354-365.

- [29] Y. Zhang, Review of the structural, magnetic and magnetocaloric properties in ternary rare earth RE_2T_2X type intermetallic compounds, *J. Alloys Compounds* 787 (2019) 1173-1186.
- [30] L. Li, M. Yan, Recent progresses in exploring the rare earth based intermetallic compounds for cryogenic magnetic refrigeration, *J. Alloys Compounds* 823 (2020) 153810.
- [31] L. Li, Y. Yuan, Y. Qi, Q. Wang, S. Zhou, Achievement of a table-like magnetocaloric effect in the dual-phase $ErZn_2/ErZn$ composite, *Materials Research Letters* 6 (2018) 67-71.
- [32] Y. Zhang, B. Wu, D. Guo, J. Wang, Z. Ren, Magnetic properties and promising cryogenic magneto-caloric performances of $Gd_{20}Ho_{20}Tm_{20}Cu_{20}Ni_{20}$ amorphous ribbons, *Chinese Physics B* 30 (2021) 017501.
- [33] J. Waybright, L. Halbritter, B. Dahal, H. Qian, Y. Huh, P. Lukashev, P. Kharel, Structure and magnetism of $NiFeMnGa_xSn_{1-x}$ ($x= 0, 0.25, 0.5, 0.75, 1.00$) Heusler compounds, *AIP Advances* 9 (2019) 035105.
- [34] P. Nehla, V. Anand, B. Klemke, B. Lake, R. Dhaka, Magnetocaloric properties and critical behavior of $Co_2Cr_{1-x}Mn_xAl$ Heusler alloys, *J. Applied Phys.* 126 (2019) 203903.
- [35] S. Ghosh, A. Ghosh, P. Sen, K. Mandal, Giant Room-Temperature Magnetocaloric Effect Across the Magnetostructural Transition in $(Mn Ni Si)_{1-x}(Fe Co Ga)_x$ Alloys, *Phys. Rev. Appl.* 14 (2020) 014016.
- [36] Y. Jin, J. Waybright, P. Kharel, I. Tadic, J. Herran, P. Lukashev, S. Valloppilly, D. Sellmyer, Effect of Fe substitution on the structural, magnetic and electron-transport properties of half-metallic Co_2TiSi , *AIP Advances* 7 (2017) 055812.
- [37] A. Ahmad, S. Srivastava, A. Das, First-principles calculations and experimental studies on Co_2FeGe Heusler alloy nanoparticles for spintronics applications, *J. Alloys Compounds* 878 (2021) 160341.
- [38] C. Felser, B. Hillebrands, New materials with high spin polarization: half-metallic Heusler compounds, *J. Phys. D: Appl. Phys.* 40 (2007) E01.
- [39] M. Obaida, L. Galdun, T. Ryba, V. Komanicky, K. Saksl, M. Durisin, J. Kovac, V. Haskova, P. Szabo, Z. Vargova, Spin polarization in Cu_2MnSn Heusler alloy produced by melt-spinning, *Intermetallics* 85 (2017) 139-143.
- [40] A. Pogorily, A. Kravets, V. Nevdacha, D. Podyalovskiy, S. Ryabchenko, V. Kalita, M. Kulik, A. Lozenko, A.Y. Vovk, M. Godinho, Magnetic anisotropy of epitaxial Co_2FeGe Heusler alloy films on $MgO(100)$ substrates, *AIP advances* 7 (2017) 055831.

- [41] R. Sahoo, A. Das, N. Stuesser, K. Suresh, Field dependent neutron diffraction study in $\text{Ni}_{50}\text{Mn}_{38}\text{Sb}_{12}$ Heusler alloy, *Appl. Phys. Lett.* 110 (2017) 021902.
- [42] L. Galdun, P. Szabo, V. Vega, E.D. Barriga-Castro, R. Mendoza-Reséndez, C. Luna, J. Kovac, O. Milkovic, R. Varga, V.M. Prida, High Spin Polarization in Co_2FeSn Heusler Nanowires for Spintronics, *ACS Applied Nano Materials* 3 (2020) 7438-7445.
- [43] C. Phatak, O. Heinonen, M. De Graef, A. Petford-Long, Nanoscale skyrmions in a nonchiral metallic multiferroic: Ni_2MnGa , *Nano Letters* 16 (2016) 4141-4148.
- [44] M. Yin, P. Nash, S. Chen, Enthalpies of formation of selected Fe_2YZ Heusler compounds, *Intermetallics* 57 (2015) 34-40.
- [45] F. Dahmane, Y. Mogulkoc, B. Doumi, A. Tadjer, R. Khenata, S.B. Omran, D. Rai, G. Murtaza, D. Varshney, Structural, electronic and magnetic properties of Fe_2 -based full Heusler alloys: A first principle study, *J. Magn. Magn. Mater.* 407 (2016) 167-174.
- [46] Y. Matsushita, G. Madjarova, J. Dewhurst, S. Shallcross, C. Felser, S. Sharma, E. Gross, Large magnetocrystalline anisotropy in tetragonally distorted Heuslers: a systematic study, *Journal of Physics D: Applied Physics* 50 (2017) 095002.
- [47] Y. Zhang, W. Wang, H. Zhang, E. Liu, R. Ma, G. Wu, Structure and magnetic properties of Fe_2NiZ ($Z = \text{Al, Ga, Si}$ and Ge) Heusler alloys, *Physica B: Condensed Matter* 420 (2013) 86-89.
- [48] D.C. Gupta, I.H. Bhat, Full-potential study of Fe_2NiZ ($Z = \text{Al, Si, Ga, Ge}$), *Materials Chemistry and Physics*, 146 (2014) 303-312.
- [49] A. Ahmad, S. Mitra, S. Biswas, S. Srivastava, A. Das, Site preferences of Fe_2CoAl Heusler alloy: A first-principles DFT study, in: *AIP Conference Proceedings*, 2115 (2019) pp. 030508.
- [50] T. Saito, D. Nishio-Hamane, Magnetic and thermoelectric properties of melt-spun ribbons of Fe_2XAl ($X = \text{Co, Ni}$) Heusler compounds, *Journal of Applied Physics* 124 (2018) 075105.
- [51] J. Du, Y. Zuo, Z. Wang, J. Ma, L. Xi, Properties of Co_2FeAl Heusler alloy nano-particles synthesized by coprecipitation and thermal deoxidization method, *Journal of Materials Science & Technology*, 29 (2013) 245-248.
- [52] A. Ahmad, S. Mitra, S. Srivastava, A. Das, Size-dependent structural and magnetic properties of disordered Co_2FeAl Heusler alloy nanoparticles, *J. Magn. Magn. Mater.* 474 (2019) 599-604.

- [53] I. Galanakis, E. Şaşlıoğlu, S. Blügel, K. Özdoğan, Voids-driven breakdown of the local-symmetry and Slater-Pauling rule in half-metallic Heusler compounds, *Physical Review B* 90 (2014) 064408.
- [54] V. Jain, J. Nehra, V. Sudheesh, N. Lakshmi, K. Venugopalan, Comparative study of the structural and magnetic properties of bulk and nano-sized Fe₂CoAl, *AIP Conference Proceedings* 1536 (2013) pp. 935-936.
- [55] S. Roy, N. Khan, R. Singha, A. Pariari, P. Mandal, Complex exchange mechanism driven ferromagnetism in half-metallic Heusler Co₂TiGe: Evidence from critical behavior, *Physical Review B* 99 (2019) 214414.
- [56] A. Arrott, Criterion for ferromagnetism from observations of magnetic isotherms, *Physical Review* 108 (1957) 1394.
- [57] B. Banerjee, On a generalised approach to first and second order magnetic transitions, *PhL*, 12 (1964) 16-17.
- [58] A.M. Tishin, Y.I. Spichkin, *The magnetocaloric effect and its applications*, CRC Press, 2016.
- [59] A. Aryal, A. Quetz, S. Pandey, T. Samanta, I. Dubenko, D. Mazumdar, S. Stadler, N. Ali, Phase transitions and magnetocaloric and transport properties in off-stoichiometric GdNi₂Mnx, *J. Appl. Phys.* 119 (2016) 043905.
- [60] K. Engelbrecht, C.R.H. Bahl, Evaluating the effect of magnetocaloric properties on magnetic refrigeration performance, *J. Appl. Phys.* 108 (2010) 123918.
- [61] H. Takeya, V. Pecharsky, K. Gschneidner Jr, J. Moorman, New type of magnetocaloric effect: Implications on low-temperature magnetic refrigeration using an Ericsson cycle, *Applied Physics Letters* 64 (1994) 2739-2741.
- [62] K. Sielicki, R. Wróblewski, M. Leonowicz, Magnetocaloric properties of stacked Ni₅₀Mn_{18.75x}Cu_{6.25+x}Ga₂₅ (x= 0; 0, 25; 0, 5) polycrystalline alloys, in, *Division of Construction and Functional Materials*, 2015.
- [63] N. Trung, V. Biharie, L. Zhang, L. Caron, K. Buschow, E. Brück, From single-to double-first-order magnetic phase transition in magnetocaloric Mn_{1-x}Cr_xCoGe compounds, *Applied Physics Letters* 96 (2010) 162507.
- [64] A. Aryal, A. Quetz, S. Pandey, I. Dubenko, S. Stadler, N. Ali, Phase transitions and magnetocaloric properties in MnCo_{1-x}Zr_xGe compounds, *Advances in Condensed Matter Physics* 2017 (2017).

- [65] A. Aryal, A. Quetz, S. Pandey, T. Samanta, I. Dubenko, M. Hill, D. Mazumdar, S. Stadler, N. Ali, Magnetostructural phase transitions and magnetocaloric effects in as-cast $\text{Mn}_{1-x}\text{Al}_x\text{CoGe}$ compounds, *Journal of Alloys and Compounds*, 709 (2017) 142-146.
- [66] A. Ahmad, S. Srivastava, A. Das, The Giant magnetocaloric effect and magnetic field induced magneto-structural phase transition in A2-disordered Co_2FeAl Heusler nanoalloy, arXiv preprint arXiv:1909.10201, (2019).
- [67] J. Panda, S. Saha, T. Nath, Critical behavior and magnetocaloric effect in $\text{Co}_{50-x}\text{Ni}_x\text{Cr}_{25}\text{Al}_{25}$ ($x= 0$ and 5) full Heusler alloy system, *Journal of Alloys and Compounds*, 644 (2015) 930-938.
- [68] S. Mathew, S. Kaul, Tuning magnetocaloric effect with nanocrystallite size, *applied physics letters*, 98 (2011) 172505.
- [69] F.-x. Hu, B.-g. Shen, J.-r. Sun, Magnetic entropy change in $\text{Ni}_{51.5}\text{Mn}_{22.7}\text{Ga}_{25.8}$ alloy, *Applied Physics Letters*, 76 (2000) 3460-3462.
- [70] M. Ghorbani Zavareh, C. Salazar Mejía, A. Nayak, Y. Skourski, J. Wosnitza, C. Felser, M. Nicklas, Direct measurements of the magnetocaloric effect in pulsed magnetic fields: The example of the Heusler alloy $\text{Ni}_{50}\text{Mn}_{35}\text{In}_{15}$, *Applied Physics Letters*, 106 (2015) 071904.
- [71] Z. Li, K. Xu, Y. Zhang, C. Tao, D. Zheng, C. Jing, Two successive magneto-structural transformations and their relation to enhanced magnetocaloric effect for $\text{Ni}_{55.8}\text{Mn}_{18.1}\text{Ga}_{26.1}$ Heusler alloy, *Scientific reports*, 5 (2015) 1-7.
- [72] J.-H. Chen, N.M. Bruno, Z. Ning, W.A. Shelton, I. Karaman, Y. Huang, J. Li, J.H. Ross Jr, Relative cooling power enhancement by tuning magneto-structural stability in Ni-Mn-In Heusler alloys, *Journal of Alloys and Compounds*, 744 (2018) 785-790.
- [73] V. Franco, J. Blázquez, A. Conde, Field dependence of the magnetocaloric effect in materials with a second order phase transition: A master curve for the magnetic entropy change, *Applied physics letters*, 89 (2006) 222512.
- [74] B. Dahal, C. Huber, W. Zhang, S. Valloppilly, Y. Huh, P. Kharel, D. Sellmyer, Effect of partial substitution of In with Mn on the structural, magnetic, and magnetocaloric properties of $\text{Ni}_2\text{Mn}_{1+x}\text{In}_{1-x}$ Heusler alloys, *Journal of Physics D: Applied Physics*, 52 (2019) 425305.
- [75] A. Kitanovski, P.W. Egolf, Innovative ideas for future research on magnetocaloric technologies, *International journal of refrigeration*, 33 (2010) 449-464.

